Published in final edited form as:
Nat Ecol Evol. 2020 April ; 4(4): 543–549. doi:10.1038/s41559-020-1122-9.

A one-billion-year-old multicellular chlorophyte

Qing Tang[1,*], **Ke Pang**[2,3], **Xunlai Yuan**[2,3], **Shuhai Xiao**[1,*]

[1]Department of Geosciences and Global Change Center, Virginia Tech, Blacksburg, Virginia 24061, USA

[2]State Key Laboratory of Palaeobiology and Stratigraphy, Nanjing Institute of Geology and Palaeontology and Center for Excellence in Life and Paleoenvironment, Chinese Academy of Sciences, Nanjing, 210008

[3]University of Chinese Academy of Sciences, Beijing 100039, China

Abstract

Chlorophytes (which represent a clade within the Viridiplantae and a sister group of the Streptophyta) probably dominated marine export bioproductivity and played a key role in facilitating ecosystem complexity before the Mesozoic diversification of phototrophic eukaryotes such as diatoms, coccolithophorans, and dinoflagellates. Molecular clock and biomarker data indicate that chlorophytes diverged in the Mesoproterozoic or early Neoproterozoic, followed by their subsequent phylogenetic diversification, multicellular evolution, and ecological expansion in the late Neoproterozoic and Paleozoic. This model, however, has not been rigorously tested with paleontological data because of the scarcity of Proterozoic chlorophyte fossils. Here we report abundant millimeter-sized, multicellular, and morphologically differentiated macrofossils from ~1,000 Ma rocks. These fossils are described as *Proterocladus antiquus* new species and are interpreted as benthic siphonocladalean chlorophytes, suggesting that chlorophytes acquired macroscopic size, multicellularity, and cellular differentiation nearly a billion years ago, much earlier than previously thought.

The origin of photosynthetic eukaryotes represents a key evolutionary innovation that ultimately precipitated in major ecosystem-wide changes in Earth history. The Archaeplastida, which includes the Rhodophyta and Viridiplantae, have been the most ecologically successful photosynthetic eukaryotes today and in geological past. Rhodophytes donated their plastids to diatoms, coccolithophorans, and dinoflagellates, which have been the dominant contributors to marine export bioproduction since the Mesozoic[1,2], whereas viridiplantae were likely the dominant export bioproducers in Paleozoic, Ediacaran, and Cryogenian oceans[3,4]. Whether viridiplantae were present before the Cryogenian Period and when they evolved multicellularity, however, is unclear. Some

* xiao@vt.edu; qingt@vt.edu.

Author Contributions Q.T. and S.X. designed the research, Q.T. and K.P. conducted fieldwork, Q.T. conducted microscopic observation. S.X. and Q.T. developed the interpretation and prepared the manuscript with input from other co-authors.

Competing interest The authors declare no competing financial interests.

recent molecular clock analyses indicate that the Rhodophyta and Viridiplantae diverged in the Paleoproterozoic–Mesoproterozoic Era[5–7], crown-group Chlorophyta (which is a clade within the Viridiplantae, a sister group of the Streptophyta, and includes prasinophytes and the core Chlorophyta[8]) diverged in the late Mesoproterozoic to early Neoproterozoic eras[6,9–11], but multicellular, siphonous, and siphonocladous chlorophytes evolved repeatedly in the late Neoproterozoic and Paleozoic[10,12]. However, these molecular clock estimates come with large uncertainties on the order of several hundred million years, particularly for early divergence events within the Archaeplastida, Viridiplantae, and Chlorophyta[6,10]. Furthermore, some of these molecular clocks give conflicting estimates; for example, the divergence of crown-group Chlorophyta is estimated to have occurred at 0.466–0.792 Ga[11] or 0.903–1.329 Ga[6], and that of crown-group embryophytes in the Cambrian[13] or Ordovician Period[10]. These problems are in part related to the scarcity of reliable fossil calibrations in the Proterozoic. Molecular clock studies had to choose between largely ignoring Proterozoic fossils or calibrating clocks against putative Proterozoic archaeplastid fossils, which are few and far between. For example, there are only a handful of Proterozoic rhodophyte fossils even in the most optimistic view, including the ~1.6 Ga *Ramathallus*[14] (but see ref.[15] that questions its rhodophyte or even archaeplastid interpretation), the ~1.05 Ga *Bangiomorpha*[7], and ~0.6 Ga florideophytes from the Doushantuo Formation[16]. Similarly, Proterozoic chlorophytes are represented by only one plausible genus, the ~0.72 Ma *Proterocladus*[17], which is preserved as fragments and thus its phylogenetic interpretation has been questioned due to the scanty morphological information[10,11,18]. The poor record of Proterozoic archaeplastid fossils means large uncertainties in their stratigraphic ranges[19], hence limiting their values as fossil calibrations in molecular clock studies. Thus, it is imperative to document Proterozoic archaeplastid fossils, particularly chlorophyte fossils, not only to improve fossil calibrations so that molecular clocks are not entirely calibrated on Phanerozoic fossils, but also to evaluate evolutionary models derived from molecular clocks[11] and fossil biomarkers[3,20–22].

Here we report a multicellular fossil, *Proterocladus antiquus* new species, that occurs in abundance in the ca. 1,000-Ma Nanfen Formation in North China (Extended Data Fig. 1). Compared with previously reported fragments of *Proterocladus*[17], the new species offers a more complete suite of morphological features—including inferred siphonocladous construction, multicellularity, and newly documented characters such as cell differentiation, a multitude of branching, and a holdfast structure—that collectively strengthen a phylogenetic position within the crown-group Chlorophyta. The new fossil indicates that chlorophytes acquired multicellularity and cell differentiation no later than the Tonian Period, and may have become phylogenetically diverse much earlier than predicted by the molecular clock data[10]. Considering the abundant occurrence of *Proterocladus* in the Nanfen Formation, chlorophytes may have played notable ecological and geobiological roles, at least locally if not globally, prior to the Cryogenian Period when their biomarkers became abundant[3].

Stratigraphic background

The late Mesoproterozoic to Neoproterozoic sedimentary sequence in southern Liaoning Province, North China, is well preserved with a maximum thickness of ~12.7 kilometers[23].

The sequence comprises, in ascending order, the Yongning, Xihe, Wuhangshan, and Jinxian groups (see “Stratigraphy and sedimentary environment” in Supplementary Information; Extended Data Fig. 1). Briefly, the Nanfen Formation, which contains the *Proterocladus* material described in this paper, is conformably sandwiched between two sandstone units of the Xihe Group, the underlying Diaoyutai Formation and the overlying Qiaotou Formation. The Nanfen Formation is divided into three members. The lower member is dominated by dark grey and yellowish green silty shale and mudstone that preserves *Proterocladus* fossils; the middle member consists of thick-bedded greyish argillaceous limestone; and the upper member is mainly composed of grey, yellowish, and purple shale with thin-bedded sandstone interbeds[24]. Although there are no reliable radiometric ages directly from the Nanfen Formation, the youngest population of detrital zircons from the underlying Diaoyutai Formation is dated at 1,056 ± 22 Ma[25], and a diabase sill emplaced in the overlying Qiaotou Formation gives a zircon SIMS U-Pb age of 947.8 ± 7.4 Ma[26]. Hence, the depositional age of the Nanfen Formation is constrained between 1,056 Ma and 947.8 Ma, consistent with numerous other radiometric ages from the Xihe, Wuxingshan, and Jinxian groups (Extended Data Fig. 1; see also “Age constraints” in Supplementary Information). Considering that the fossiliferous horizon of *Proterocladus* is in the lower member of the Nanfen Formation, the first occurrence of *Proterocladus* is likely near the Mesoproterozoic–Neoproterozoic boundary, or ca. 1,000 Ma.

Results

Systematic Paleontology

Phylum Chlorophyta Pascher, 1914 (ref. [27])

Class Ulvophyceae Mattox and Stewart, 1984 (ref. [28])

Order Siphonocladales (Blackman & Tansley) Oltmanns, 1904 (ref. [29])

Genus *Proterocladus* Butterfield *in* Butterfield et al., 1994 (ref. [17]), emended

Type species.—Proterocladus major Butterfield *in* Butterfield et al., 1994

Emended diagnosis.——Thallus consisting of multicellular, uniseriate, and branching filaments with intercellular septa. Filaments are typically constricted at septa. Branches typically emanate laterally from a cell in the central axis and subjacent to a septum. Lateral branches themselves can be septate. Maximally one branch per cell. Multiple orders of branches can occur, resulting in apical or upward growth. A sub-discoidal holdfast may be present. Cells typically elongate, thin-walled, mostly cylindrical, but globose, clavate, cyathiform, and doliform hetermorphic cells are occasionally present. Cell width gradually increases distally (or adapically). Apical cells round or capitate, sometimes bearing a narrow extension at the distal end.

Remarks.——*Proterocladus* was first erected by Butterfield[17] based on fragmentary materials from the late Tonian Svanbergfjellet Formation in Svalbard. Abundant well-preserved specimens of *Proterocladus* from the Nanfen Formation reveal new diagnostic

features of the genus, including variations of cell shape and cell size, multiple orders of lateral branches, upward growth, apical extension, and sub-discoidal holdfast. Thus, the genus diagnosis is here emended to accommodate these features.

Proterocladus has been compared with extant siphonocladalean *Cladophoropsis* because of their morphological similarity[17]. Indeed, both taxa are characterized by a distinctive branching pattern wherein a lateral branch emanates from the main axis subjacent to a septum. However, this branching pattern is not unique to *Cladophoropsis*; it is also present in other siphonocladaleans, such as *Cladophora* and *Rhizoclonium*[30,31]. More importantly, although they all can have regular intercalary cell divisions and thus centripetal invagination[32,33], some *Cladophoropsis* species can occasionally have segregative cell division and usually develop tenacular cells as an attachment structure[33]. However, no *Proterocladus* specimens show a sign of segregative cell division or tenacular cells (Supplementary Table 1). In this regard, *Proterocladus* is morphologically more similar to *Cladophora* (e.g., *C. herpestica*[33]) and *Rhizoclonium* (e.g., *R. ramosum*[30]) than to *Cladophoropsis*. Regardless, the extant Siphonocladales provides the best interpretative analog for *Proterocladus*, suggesting that *Proterocladus* may be a member of the total-group Siphonocladales. A more detailed discussion of the phylogenetic affinity of *Proterocladus* is presented in the discussion section.

Proterocladus is superficially similar to *Aimonema* Hermann *in* Hermann and Podkovyrov, 2010 (ref. [34]), an articulated form of *Palaeovaucheria* Hermann, 1981 (ref. [35]), in having a branching thallus and clavate terminal cells. However, *Proterocladus* is distinguished from *Aimonema* and *Palaeovaucharia* in its apical or upward branching pattern and discoidal holdfast, whereas *Aimonema* has a reticulate thallus similar to extant nematode-trapping fungi[34]. Additionally, filamentous algal fragments from the Middle Ordovician Winneshiek Shale are similar to *Proterocladus* in having a *Cladophora*-style branching system[36]. However, their cells are much larger than those of *Proterocladus* (90–380 μm vs. 6–35 μm in cell width), although the Winneshiek fossils may represent a younger record of siphonocladalean chlorophytes[36].

The organic-walled microfossil *Jacutianema* is morphologically similar to *Proterocladus* in having side branches adjacent to one end of the mother cell and possible siphonous/siphonocladous construction[17]. Given that *Jacutianema* co-occurs with *Proterocladus* in the Svanbergfjellet Formation of Svalbard, an interesting hypothesis is that *Jacutianema* may represent the akinete of *Proterocladus*, and this hypothesis needs to be investigated further by a detailed restudy of the Svalbard material. Additionally, branching thalli from the ca. 1,078 Ma Nonesuch Formation (fig. 2L, M of ref. [37]) are morphologically similar to fragmented specimens of *Proterocladus* in the Nanfen Formation (e.g., Fig. 2b, d), suggesting that they may represent broken pieces of *Proterocladus*. However, more completely preserved specimens from the Nonesuch Formation are needed in order to confirm their taxonomic identification as *Proterocladus*.

Occurrence.——*Proterocladus* has been recovered from latest Mesoproterozoic to Tonian successions, including the late Tonian Svanbergfjellet Formation in Svalbard[17], the late Tonian Khastakh Formation in Siberia[38], the latest Mesoproterozoic to early Tonian Nanfen

Formation in North China, and possibly the latest Mesoproterozoic Nonesuch Formation in North America[37].

Proterocladus antiquus new species

2018 *Proterocladus* sp.; Xiao and Tang [39], fig. 3B.

Holotype.——VPIGM-4762 in Fig. 2g, reposited at Virginia Polytechnic Institute Geoscience Museum.

Paratype.——VPIGM-4799 in Fig. 1l, reposited at Virginia Polytechnic Institute Geoscience Museum.

Diagnosis.——A species of *Proterocladus* characterized by a differentiated sub-discoidal holdfast, morphologically distinct akinetes, multiple orders of lateral branches constructing an upward-growing thallus, and an apical extension. Cells defined by robust septa and associated constrictions. Cell shape and size are variable in a thallus.

Etymology.——Species epithet derived from Latin, *antiquus*, referring to the Proterozoic age of the species.

Material.——1,028 specimens from the lower Nanfen Formation in North China.

Occurrence.——*Proterocladus antiquus* has been recovered from the latest Mesoproterozoic to early Tonian Nanfen Formation in North China.

Description.——Well-preserved specimens of *P. antiquus* consist of a branching thallus and a holdfast (Fig. 1a). The thallus, 0.3–3.3 mm and 0.1–2.4 mm in maximum height and width respectively, consists of uniseriate filaments that branch sparsely or profusely (Fig. 1; Extended Data Fig. 2). Branches are laterally and asymmetrically inserted, and are alternately or unilaterally arranged along the main axis (Fig. 1; Extended Data Fig. 2). The main axis and branches tend to widen distally (Fig. 1a, b, f, h, i). Lateral branches grow apically or upward and away from the insertion point (Fig. 1a, h–k). Multiple orders of lateral branches can occur (Extended Data Fig. 3a), leading to complex thallus with numerous branches and aggregates (Extended Data Fig. 3b–d). The rarely preserved holdfast is lobate or sub-discoidal in shape and 53–57 μm in maximum dimension (Fig. 1a, l; Extended Data Fig. 4).

The thallus of *P. antiquus* comprises multiple cells that are defined by complete septa (Figs. 1a; 2a–d). A constriction typically occurs at a septum, such that cell boundaries can also be recognized by constrictions when septa are poorly preserved (Figs. 1a, i, k; 2c). Cells are 14–510 μm (average = 123 μm; s.d. = 0.45; n = 321) and 6–49 μm (average = 25 μm; s.d. = 0.12; n = 321) in length and width, respectively, with a length/width ratio 0.9–26.9. They are mostly thin-walled and cylindrical in shape (Figs. 1a, i; 2a–d), but heteromorphic cells are also observed occasionally (Fig. 1a), including globose (Fig. 1j, k; Extended Data Fig. 5a–c), clavate (Figs. 1j; 2e; Extended Data Fig. 5d–f), doliform (Fig. 2f–h; Extended Data Fig. 5g–k), and cyathiform cells (Figs. 1c, g, i; 2a, i, j; Extended Data Fig. 5l). These

heteromorphic cells are also distinctive in their greater maximum cell width and nearly opaque cell-wall (Figs. 1b, j; 2g, h, j), suggesting thicker or more recalcitrant cell walls. Some cells appear to have a minute lateral pore (Figs. 1a; 2e; Extended Data Fig. 5m–o). Lateral branches are always developed subjacent to a septum, either freely communicating with the parent cell (Figs. 1a, i–l; 2, b; Extended Data Figs. 5g, l; 6) or separated from the mother cell by a septum at the branching point (Figs. 1a, j, l; 2b, f). Some terminal cells have a distinct narrow apical extension (Figs. 1a, e, i; 2a, j, k; Extended Data Fig. 6d), possibly representing apical cell division, which is supported by the development of septa in presumably more mature apical extensions (Extended Data Figs. 6e; 7).

Remarks.——The type species *Proterocladus major*, along with two other species of *Proterocladus—P. minor and P. hermannae*, was erected based on fragmentary specimens from the late Tonian Svanbergfjellet Formation in Svalbard[17]. The new species *P. antiquus* is distinguished from other species of *Proterocladus* in the presence of a holdfast, akinetes, multiple orders of lateral branches that grow upward, and an apical extension. However, given that the type species *P. major* was erected on the basis of fragmentary specimens, it is possible that *P. antiquus* and *P. major* are synonymous as some fragments of *P. antiquus* appear identical to *P. major*.

Proterocladus major, *P. minor*, and *P. hermannae* were distinguished by their cell size, the prominence of constrictions, and the frequency of septa[17]. However, our investigation on a large collection of well-preserved specimens of *P. antiquus* in the Nanfen Formation shows that cell width can vary gradually from the base to the top of the thallus (e.g. Fig. 1b, f, i, j). Thus, cell size alone is probably not a reliable criterion to differentiate species of *Proterocladus*, particularly if they are preserved as fragments. The frequency of intercellular septa and constrictions is also variable, as indicated by the highly variable cell length measurements. Thus, if *P. antiquus* and *P. major* are synonymous, it is possible that all four known species of *Proterocladus* are synonymous. This possibility needs to be evaluated by a restudy of the Svanbergfjellet material and the discovery of more completely preserved specimens of *Proterocladus* from the Svanbergfjellet Formation. At the present, to preserve taxonomic objectivity and to highlight the morphological complexity as revealed by the well-preserved Nanfen material, we choose to place the Nanfan material in *Proterocladus antiquus* new species. In addition, the *Proterocladus* specimen reported in ref. [39] is here regarded as *P. antiquus* given that it was recovered from the same horizon of *P. antiquus* reported in this study.

Discussion

The well-preserved specimens of *P. antiquus*, which is broadly similar to and could even be synonymous with the type species *P. major* from Svalbard (see “Systematic paleontology”), reveal a suite of features that were not preserved in the fragmentary material of *P. major* but can assist in the morphological reconstruction as well as ecological and phylogenetic interpretations of *Proterocladus*. Specifically, the more opaque and larger-sized heteromorphic cells may represent specialized akinetes that form in unfavorable conditions, typically with a larger cell size and a thicker cell wall enclosing condensed cytoplasm[40] (Fig. 3a, b). The lateral pore (Figs. 1a; 2e; Extended Data Fig. 5m–o) is identical to lateral

openings of reproductive cells (e.g., gametangia and sporangia) where gametes and spores are released through such openings (Fig. 3c; fig. 10 of ref. [30]). The swollen apical cell with a narrow apical extension (Figs. 1e, i; 2g, j, k; Extended Data Fig. 6d) indicates that thallus growth was mainly achieved by apical growth, an interpretation supported by the subsequent development of septa in the apical extension at maturation (Extended Data Figs. 6e; 7). In addition, the presence of a holdfast and evidence for apical growth suggest that *Proterocladus* had an erect epibenthic habit. The dense branching pattern and the formation of aggregates suggest that *Proterocladus* likely formed tufts, which may have facilitated its colonization on the ocean floor (Fig. 4). This is also consistent with the massive preservation of *Proterocladus* in the Nanfen mudstone (Extended Data Figs. 8, 9). More importantly, the co-occurrence of extremely large cells (up to several hundred μm long; e.g., Fig. 2g) and small cells (dozens of μm long; e.g., Fig. 2g) in the same thallus indicates that the larger cells were likely coenocytic and thus *Proterocladus* was a siphonocladous (i.e., coenocytic and multicellular) organism[17]. Therefore, well-preserved Nanfen specimens indicate that *Proterocladus* was an erect epibenthic multicellular organism with filamentous branches, a unique branching pattern with asymmetrical lateral branches arising subjacent to septa, a differentiated holdfast, differentiated heteromorphic akinete-like cells, reproductive cells as inferred from the presence of lateral pores, and an inferred siphonocladous construction (Fig. 1a).

The morphological reconstruction described above are useful in phylogenetic inference of *Proterocladus* (see Supplementary Table 1). Specifically, its branching style, differentiated cells, the presence of a holdfast, inferred siphonocladous construction, and the lack of a common outer sheath place *Proterocladus* in the kingdom of Eukarya. Some stigonematalean cyanobacteria, such as *Nostochopsis* and *Thalpophila*, can develop uniseriate trichomes with differentiated akinetes, true branches, and apical growth[41]. However, stigonematalean trichomes are always surrounded by a robust outer sheath, which has reasonably good preservation potential[42] but is not present in *Proterocladus*. More importantly, no stigonematalean cyanobacteria are known to develop siphonocladous construction. To the best of our knowledge, no bacteria or archaebacteria are known to have the combination of features present in *Proterocladus* (Supplementary Table 1).

Although coenocyte or syncytium exists in many groups of eukaryotes[43], a filamentous siphonocladous construction is characteristic of only a handful of extant eukaryote groups, including some filamentous fungi (e.g., *Neurospora*[44]), xanthophytes (e.g., *Vaucheria* in reproductive stage[45]), rhodophytes (e.g., *Griffithsia*[46]), and chlorophyte (e.g., *Rhizoclonium*[30]). The vegetative structure of multinucleate fungi, septate hyphae, could be morphologically similar to *Proterocladus* in having large cells and lateral branches that sometimes adjacent to a septum[44,47]. However, fungal septa are very different from the complete septa of *Proterocladus* in that they are perforated[47]. More importantly, septate hyphae usually consist of cells with a relatively uniform size and tend to form a complex network of branching structure (i.e., mycelium), the hyphae themselves do not differentiate into a filamentous holdfast, and fungal cells can fuse to form loops of various shapes[44,48]. In addition, the reproductive organs of multinucleate fungi (such as sporangium, zygospore, ascus, conidia[47]) are also markedly different from the reproductive

cells observed in *Proterocladus*. Therefore, given its morphological differences from extant fungi, *Proterocladus* is unlikely a fungus.

The xanthophycean alga *Vaucheria* is morphologically similar to *Proterocladus* in developing apical extensions[49]. However, vegetative thallus of *Vaucheria* is siphonous (i.e., coenocytic but unicellular). Septation in *Vaucheria* only occurs in the reproductive stage at the apical end of filaments where akinetes or zoospores are produced as either detached individuals or loose chains with constricted connections in a filament sheath[45]. These features are conspicuously different from those of *Proterocladus*, where septation occurs intercalary along the entire filament.

Some uniseriate filamentous rhodophytes, such as *Griffithsia*[50], can develop siphonocladous construction, but their intercellular septa are usually characterized by pit plugs which are different from the complete septa of *Proterocladus*[17] (Fig. 2a–c; Extended Data Fig. 6a, b). More importantly, the unique branching pattern of *Proterocladus*, characterized by lateral branches originating subjacent to a septum, is distinct from the dichotomous or trichotomous branching pattern of siphonocladous rhodophytes. Thus, *Griffithsia* is not a morphological analog of *Proterocladus*.

To the best of our knowledge, modern siphonocladalean chlorophytes provide the most appropriate morphological analog of *Proterocladus*. Among uniseriate filamentous chlorophytes, siphonocladous construction is most common in the class Ulvophyceae, particularly in the order Siphonocladales (= Cladophorales and is the preferred name for this group of chlorophytes according to ref.[50]). Importantly, the initiation of lateral branches as outpocketing structures always subjacent to a septum is a key feature among extant siphonocladaleans such as *Cladophora* and *Rhizoclonium*[30,31] (Fig. 3d). Indeed, in addition to siphonocladous construction and the unique branching pattern, *Proterocladus* also shares with *Cladophora* and *Rhizoclonium* a number of other morphological features, including a holdfast and an epibenthic habit, intercalary cell division with centripetal invagination as indicated by constrictions at septa, as well as differentiated cells with lateral pores likely representing sexually reproductive cells[51] (Supplementary Table 1). Thus, among all morphological analogs discussed above, *Proterocladus* compares best with siphonocladaleans, and their morphological similarities are suggestive of a phylogenetic relationship. Of course, we cannot rule out the possibility that *Proterocladus* may represent an extinct group of siphonocladous eukaryotes that independently evolved a siphonocladalean-style branching pattern, but the Occam's razor leads us to hypothesize that *Proterocladus* is a possible siphonocladalean chlorophyte.

If our interpretation is correct, then *Proterocladus antiquus* from the ca. one-billion-year-old Nanfen Formation represents one of the earliest known multicellular chlorophytes. Chlorophyte fossils are key to test various molecular clock estimates of the origin of primary plastids and the crown-group Archaeoplastida, which range from ca. 1,900 Ma[6] to 900 Ma[52]; the divergence of crown-group Viridiplantae and Chlorophyta, which probably occurred in the Mesoproterozoic–Tonian[6,9,10]; and the internal divergences within the Chlorophyta, which were proposed to have occurred in the late Neoproterozoic and Paleozoic[10,12]. If the ca. 1,047 Ma fossil *Bangiomorpha* is accepted as a rhodophyte[51],

the divergence between the Rhodophyta and Viridiplantae must have occurred no later than the late Mesoproterozoic[7]. But the Proterozoic fossil record of the Viridiplantae and particularly the Chlorophyta is sparse and controversial at best. Various Proterozoic fossils have been interpreted as potential chlorophytes, including some Paleoproterozoic leiosphere acritarchs[53], Tonian macrofossils such as *Chuaria*, *Longfengshania*, *Protoarenicola*, *Pararenicola*, and *Parmia*[39], and the late Tonian colonial microfossil *Palaeastrum*[54]. However, the morphological simplicity of these taxa means that diagnostic chlorophyte features are few and subject to evolutionary convergence[54,55]. The interpretation of *Proterocladus* as a chlorophyte and specifically as a siphonocladalean has also been questioned[10,11,18], largely on the basis of its morphological simplicity[54,56]. Compared with previously described specimens of *Proterocladus*[17], the new material reported here offers additional phenotypic features—including a differentiated holdfast, akinetes, siphonocladous organization, and distinct branching pattern—that strengthen a morphological comparison and suggest a phylogenetic affinity with siphonocladalean chlorophytes (Supplementary Table 1). If this phylogenetic interpretation is confirmed, *Proterocladus* provides a minimum age calibration for the origin of photosynthetic eukaryotes[6,52], the divergence between the Rhodophyta and Viridiplantae[7], the internal divergences within the Chlorophyta[8,10,57,58] and even the Ulvophyceae[59], and the evolution of multicellularity and siphonocladous construction in the Chlorophyta[43,60]. Thus, *Proterocladus* suggests that the Chlorophyta may have diverged nearly a billion years ago, consistent with some molecular clock analyses[6] but not others[11,10,12].

The abundant occurrence of *Proterocladus* in the Nanfen Formation indicates that chlorophytes may have played important ecological and geobiological roles at least locally. It has been postulated that the pre-Cryogenian oceans were stratified in redox condition due to the lack of metazoans and the dominance of cyanobacterial phytoplankton as primary producers[61]. This postulation is mostly grounded on the earliest known chlorophyte and sponge biomarkers, which suggest that chlorophytes and filter-feeding metazoans diversified in the Cryogenian Period[3,62,63]. However, the abundant occurrence of chlorophytes such as *Proterocladus* in the ca. one-billion-year-old Nanfen Formation and other Mesoproterozoic–Tonian rocks, including the late Tonian Svanbergfjellet Formation in Svalbard[17], the late Tonian Khastakh Formation in Siberia[38], and possibly the latest Mesoproterozoic Nonesuch Formation in North America[37] (see ”Systematic paleontology”), indicates that macroscopic chlorophytes may have had more than a local impact on the Tonian ecosystem. Benthic macroscopic algae such as *Proterocladus* are expected to contribute markedly to local bioproductivity and organic carbon burial in coastal environments[64], to foster a myriad of ecological habits through the formation and ecological engineering of algal turfs (e.g., Fig. 4; Extended Data Figs. 3d; 8), and to facilitate the ecological complexity and diversification of eukaryotes in Tonian oceans. Therefore, together with other Tonian evolutionary innovations, such as nitrogen fixing heterocystous cyanobacteria, biomineralization, eukaryovorous predation[39], emergence of fungi[65], and perhaps the origin of animals[66], the rise of multicellular chlorophytes such as *Proterocladus* may have had a transformative impact on oceanic redox structures[67] and ecosystem complexity[1]. The ecological and geobiological roles of Tonian chlorophytes can be further tested by more focused search for stigmastane, a possible chlorophyte biomarker, in abundantly

fossiliferous units such as the Nanfen Formation. Currently available biomarker data indicate that the transition from bacterium- to eukaryote-dominated marine primary producers occurred sometime between 1,100 Ma[21] and 780–729 Ma[20,22], and the 1,047 Ma red algal fossil *Bangiomorpha*[7] and the ~1,000 Ma green algal fossil *Proterocladus* reported here are consistent with this scenario.

Methods

Fossil collection and extraction.

Proterocladus specimens are abundant in the lower Nanfen Formation (Extended Data Fig. 8). They are preserved as carbonaceous compressions on the bedding surface (Extended Data Fig. 9a–d). They are typically concentrated in thin and relatively dark-colored fossiliferous layers, which contrast with the intervening light-colored layers with sparse occurrence of fossils (e.g. Extended Data Fig. 9e–i). Totally 1,028 specimens of *Proterocladus*, including 301 well-preserved specimens discovered on bedding surfaces and 727 specimens extracted from the rock matrix using the HF acid maceration technique[71], were collected from mudstone/shale of the basal to lower Nanfen Formation.

Optical and electron microscopic analyses.

Extracted specimens were examined using an Olympus CX41 biomicroscope. Well-preserved specimens on bedding surfaces were examined using an Olympus SZX7 stereomicroscope. Both microscopes were connected with an Infinity 1 camera, which was used to photograph the fossils. Selected specimens were further analyzed using backscattered electron scanning electron microscopy (BSEM), energy dispersive X-ray spectroscopy (EDS), and EDS element mapping at the Virginia Tech Institute of Critical Technology and Applied Science Nanoscale Characterization and Fabrication Laboratory. These tests were conducted on a FEI QUANTA 600FEG environmental scanning electron microscope with a pole piece backscattered electron solid-state detector, a secondary electron Everhart-Thornley detector, and a Bruker EDX with a silicon drifted detector. BSEM specimens were coated with a ~20 nm conductive gold-palladium layer. The operating voltage in BSEM and EDS modes was 20 kV in high-vacuum condition.

Data availability

All specimens illustrated in this paper are reposited and available at Virginia Polytechnic Institute Geoscience Museum (Blacksburg, Virginia, USA; museum catalog numbers VPIGM-4749 to 4794 and VPIGM-4799).

Extended Data

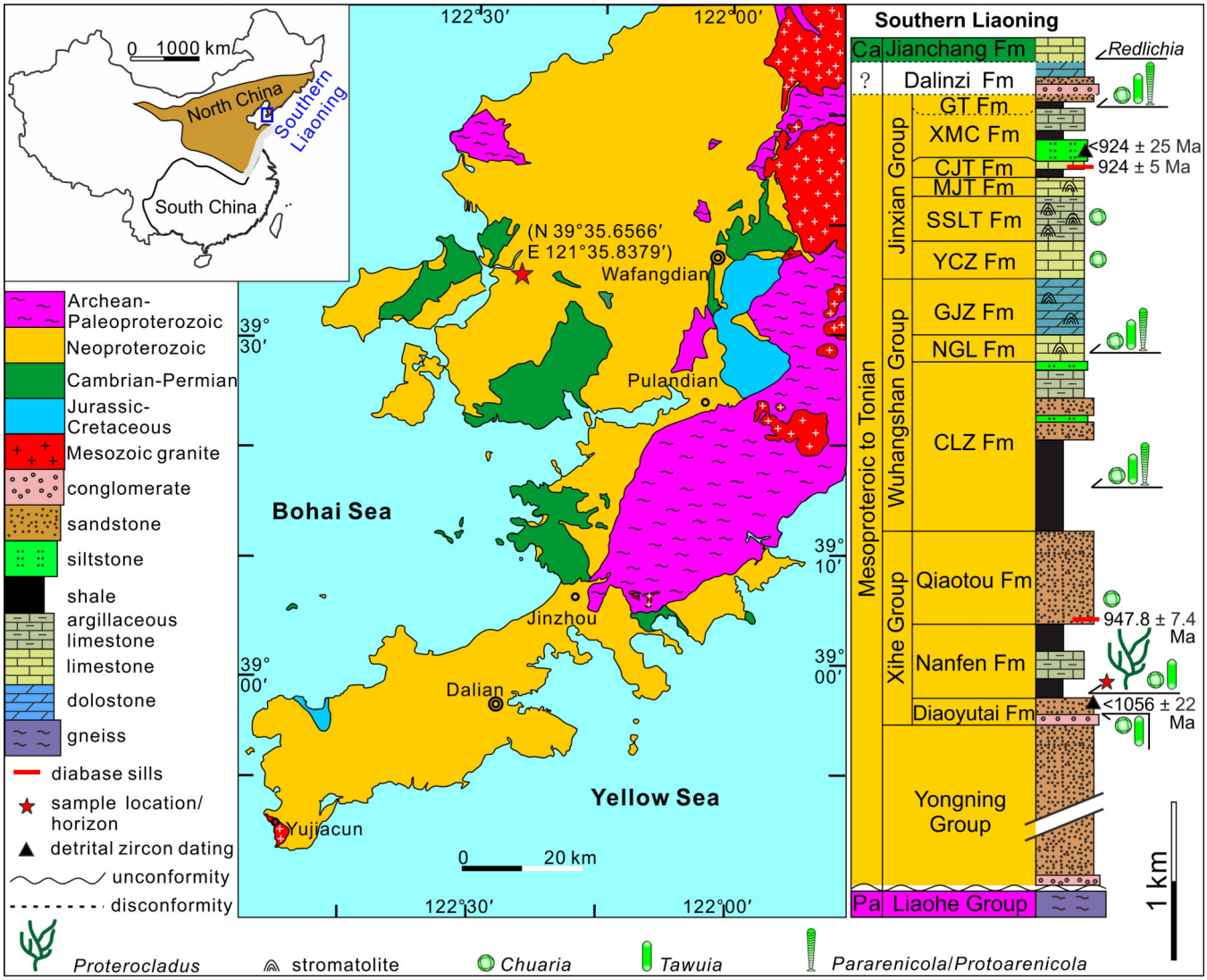

Extended Data Fig. 1. Geological map and stratigraphic column of Proterozoic successions in southern Liaoning Province, North China.

Question mark in stratigraphic column denotes poor age constraint on the Dalinzi Formation, which could be either Neoproterozoic or Cambrian in age. Stars in geological map and stratigraphic column mark sample locality (near Shileicun, 39°35.6566'N, 121°35.8379'E) and sample horizon, respectively. Ca = Cambrian, Pa = Paleoproterozoic, Fm = Formation, CLZ = Changlingzi, NGL = Nanguanling, GJZ = Ganjingzi, YCZ = Yingchengzi, SSLT = Shisanlitai, MJT = Majiatun, CJT = Cuijiatun, XMC = Xingmincun, GT = Getun. Radiometric ages (924 ± 5 Ma and 947.8 ± 7.4 Ma) of diabase sills emplaced in the Cuijiatun and Qiaotou formations are from ref. [22] and ref. [25]; detrital zircon ages (<924 ± 25 Ma and <1056 ± 22 Ma) are from ref. [24]. See ref. [25] for a compilation of ratiometric ages from Neoproterozoic successions in North China. Geological map drawn by authors based on ref. [22] with permission, and stratocolumn drawn by authors.

Extended Data Fig. 2. *Proterocladus antiquus* new species on bedding surface, showing lateral branches.

a–f, VPIGM-4763, VPIGM-4764, VPIGM-4765, VPIGM-4766, VPIGM-4767, and VPIGM-4768, respectively. All photos taken by authors.

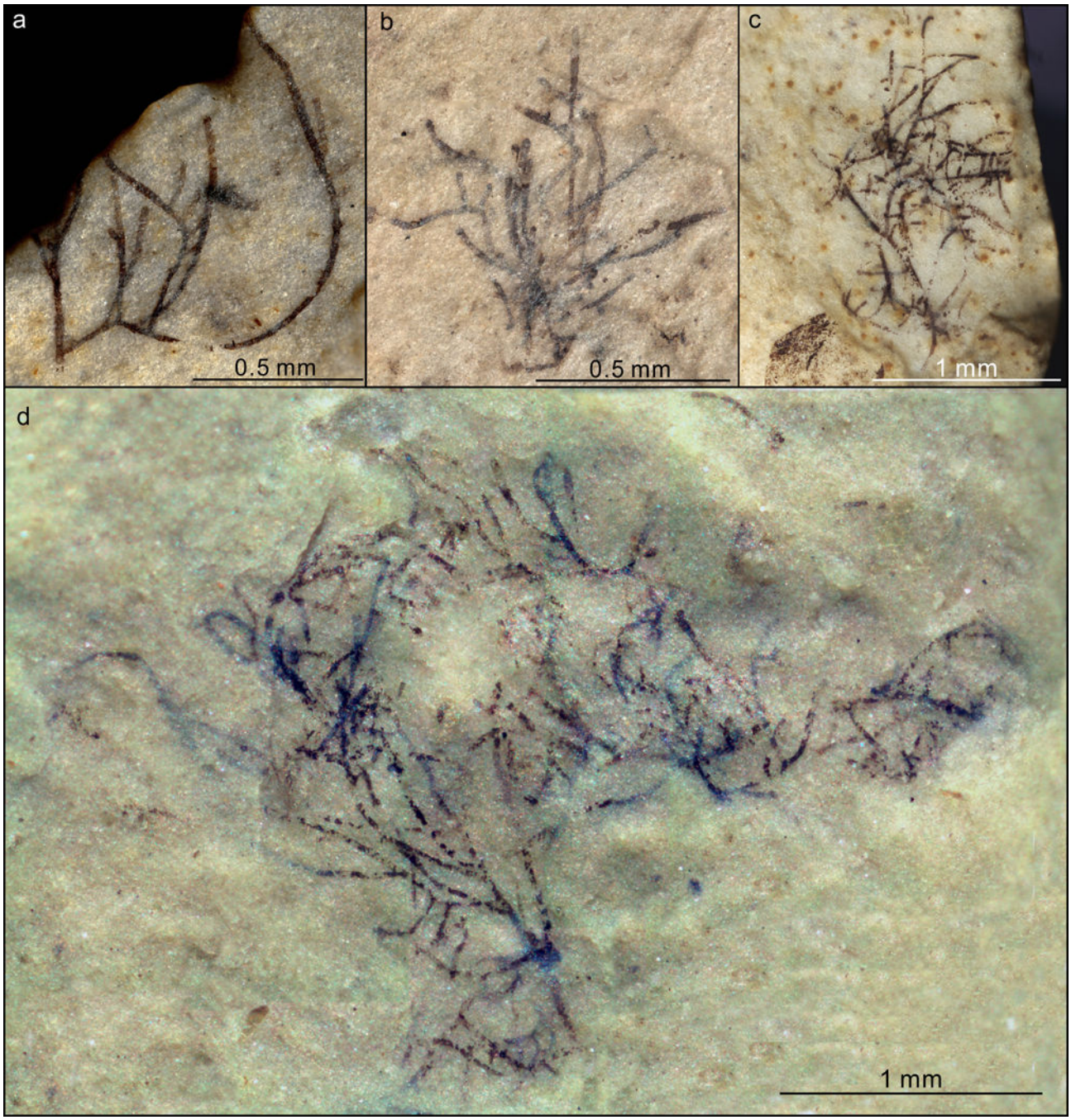

Extended Data Fig. 3. *P. antiquus* preserved on bedding surface, showing multiple orders of lateral branches (a) and aggregates of thalli (b–d).

a–d, VPIGM-4769, VPIGM-4770, VPIGM-4771, and VPIGM-4772, respectively. All photos taken by authors.

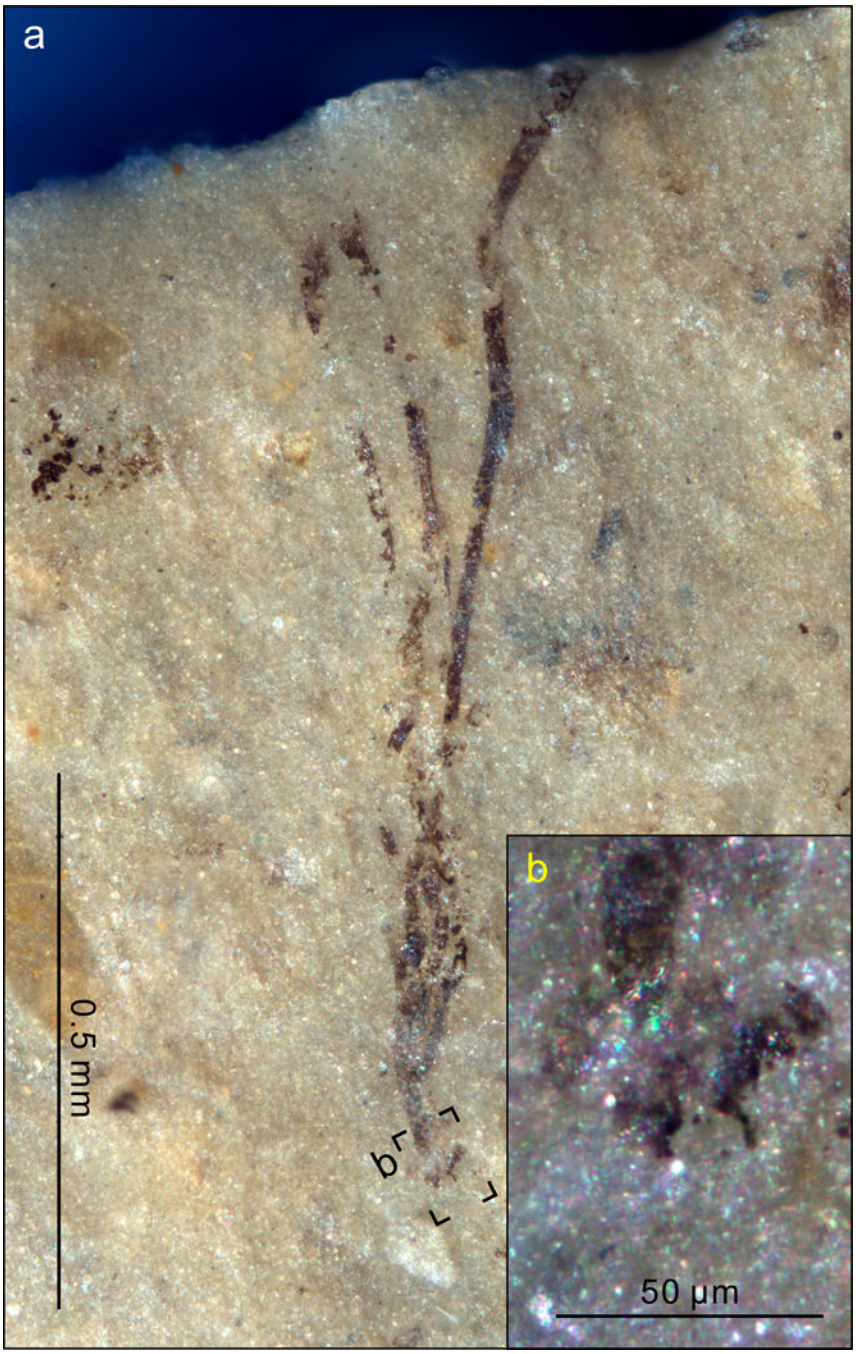

Extended Data Fig. 4. Thallus of *P. antiquus* with a sub-discoid holdfast preserved on bedding surface.

b is a close-up view of labeled black frame in **a.** VPIGM-4773. All photos taken by authors.

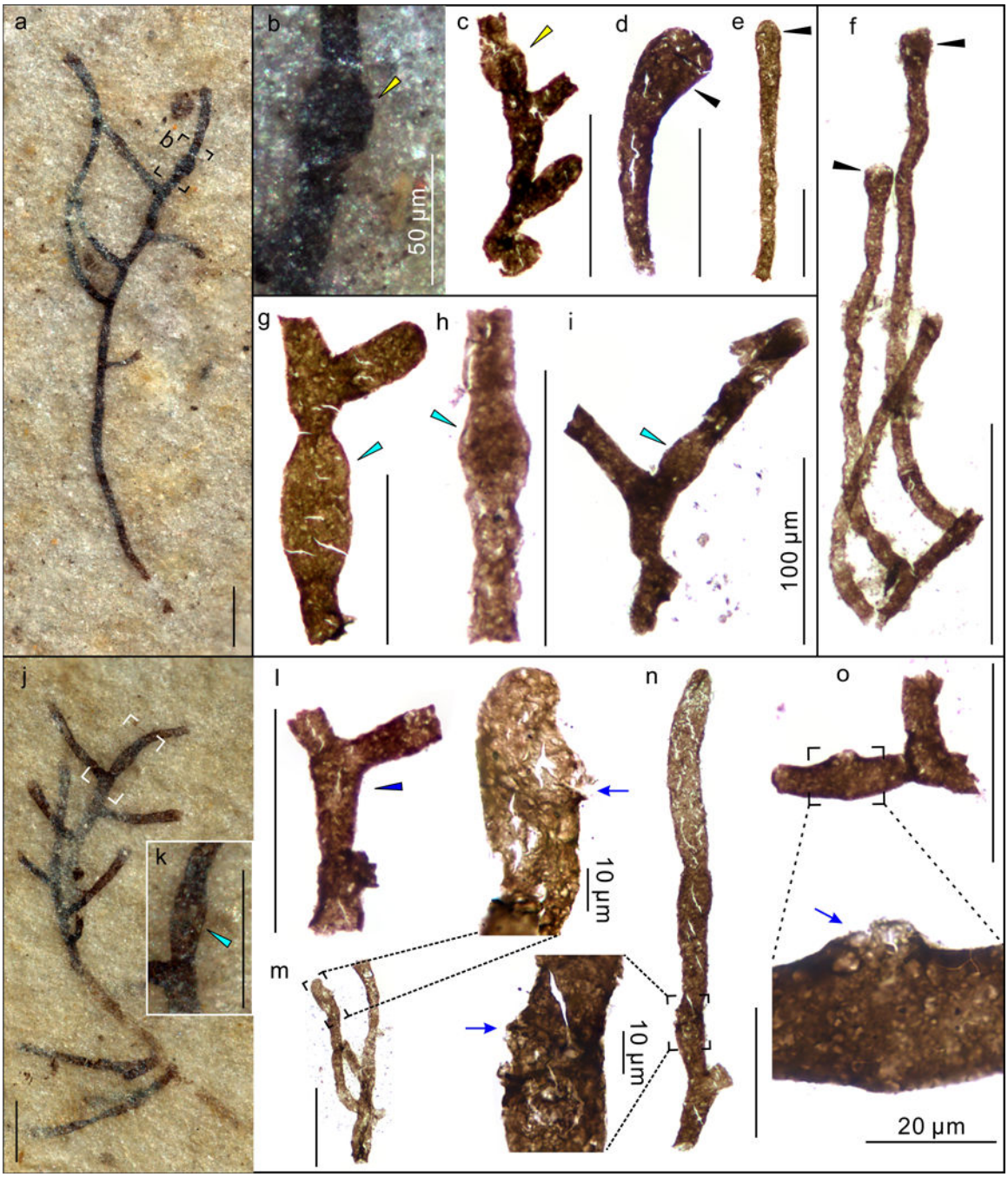

Extended Data Fig. 5. Heteromorphic cells (a–l) and reproductive cells (m–o) of *P. antiquus*.
a–l, Filaments with globose (yellow arrowheads), clavate (black arrowheads), doliform (cyan arrowheads), and cyathiform (blue arrowhead) heteromorphic cells. **b, k** are magnifications of labeled frames in **a** and **j**, respectively. VPIGM-4774, VPIGM-4775, VPIGM-4776, VPIGM-4777, VPIGM-4778, VPIGM-4779, VPIGM-4780, VPIGM-4781, VPIGM-4782, and VPIGM-4783, respectively. **m–o**, Inferred reproductive cells with minute lateral pores (blue arrows), possibly representing openings through which reproductive gametes or zoospores were released. VPIGM-4784, VPIGM-4785, and VPIGM-4786,

respectively. Specimens in **a** and **j** were photographed on bedding surface, and all other specimens were extracted from the rock matrix using HF acid maceration technique. All scale bars equal 100 μm unless otherwise specified. All photos taken by authors.

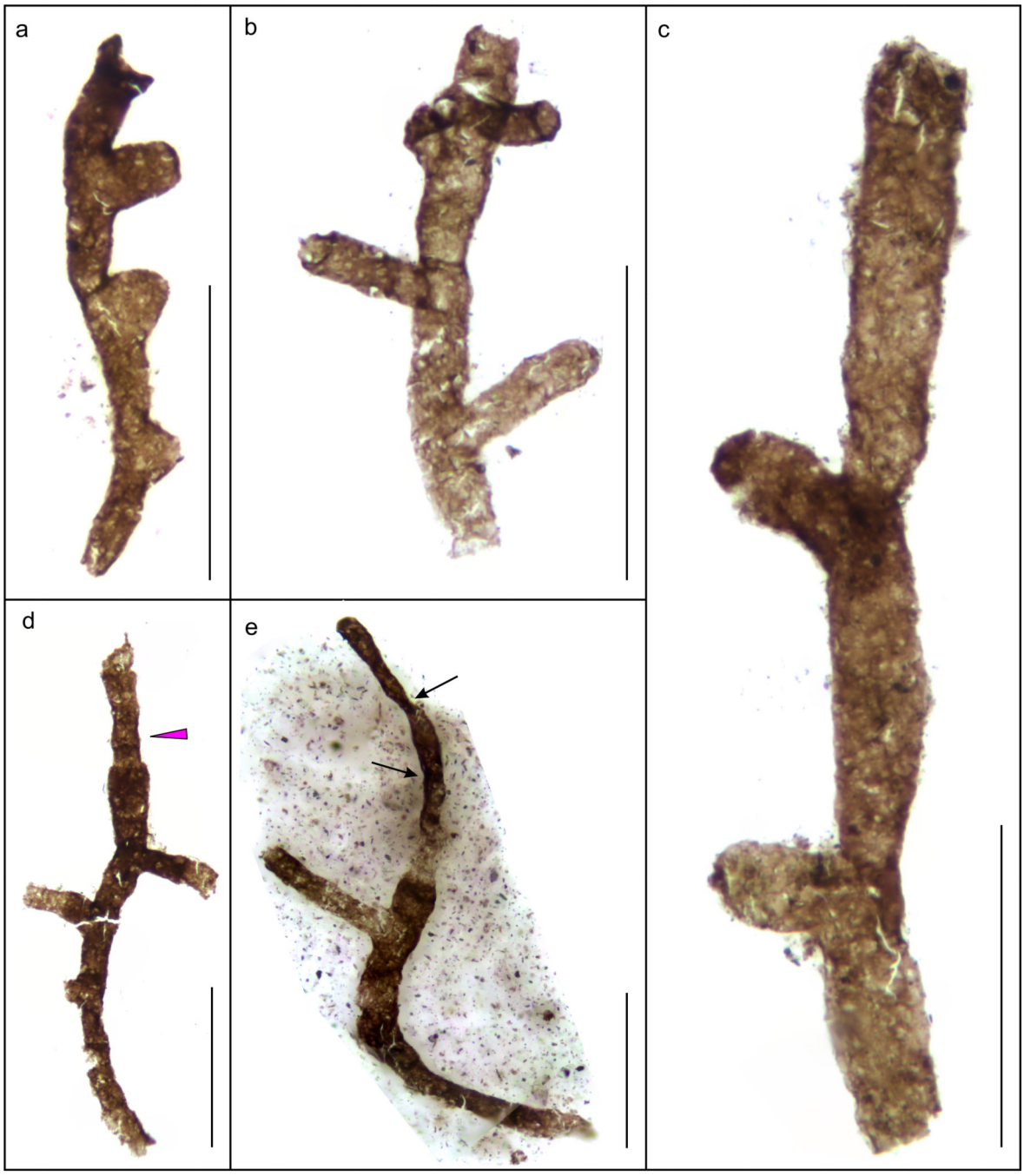

Extended Data Fig. 6. Cell branching pattern and apical extensions in extracted specimens of *P. antiquus*.

a–c, Fragmented filaments with unilateral (**a**, **c**) and alternate branches (two lower lateral branches in **b**). VPIGM-4787, VPIGM-4788, and VPIGM-4789, respectively. **d–e**, Branching filaments with an inflated apical cell subtending a narrower apical extension

(purple arrowhead in **d**) and an apical cell with septum and constriction (black arrows in **e**), which is interpreted to have developed from an apical extension. VPIGM-4790 and VPIGM-4791, respectively. All scale bars equal 100 μm. All photos taken by authors.

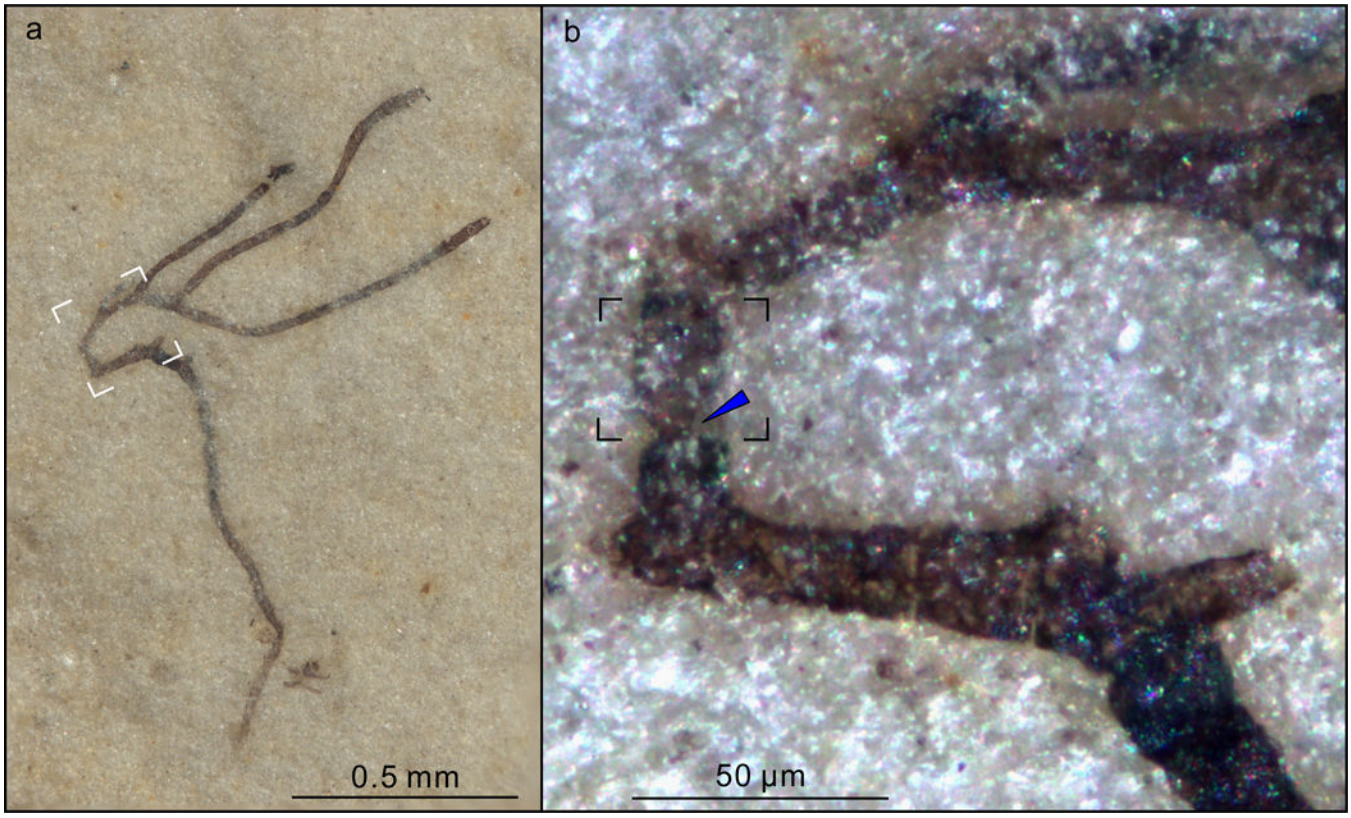

Extended Data Fig. 7. Branching thallus of *P. antiquus* with a cell (in black frame) that has a distinct constriction at base (blue arrowhead).

The branching pattern is superficially similar to H-shaped branching in the early vascular plant *Zosterophyllum*[73]. **b** is a magnification of white box in **a**, showing the basal constriction of the cell that initially may represent an apical extension that subsequently develops septa and branches at maturation. VPIGM-4792. All photos taken by authors.

Extended Data Fig. 8. Dense population of fragmented *P. antiquus* specimens preserved on bedding surface.

VPIGM-4793. All photos taken by authors.

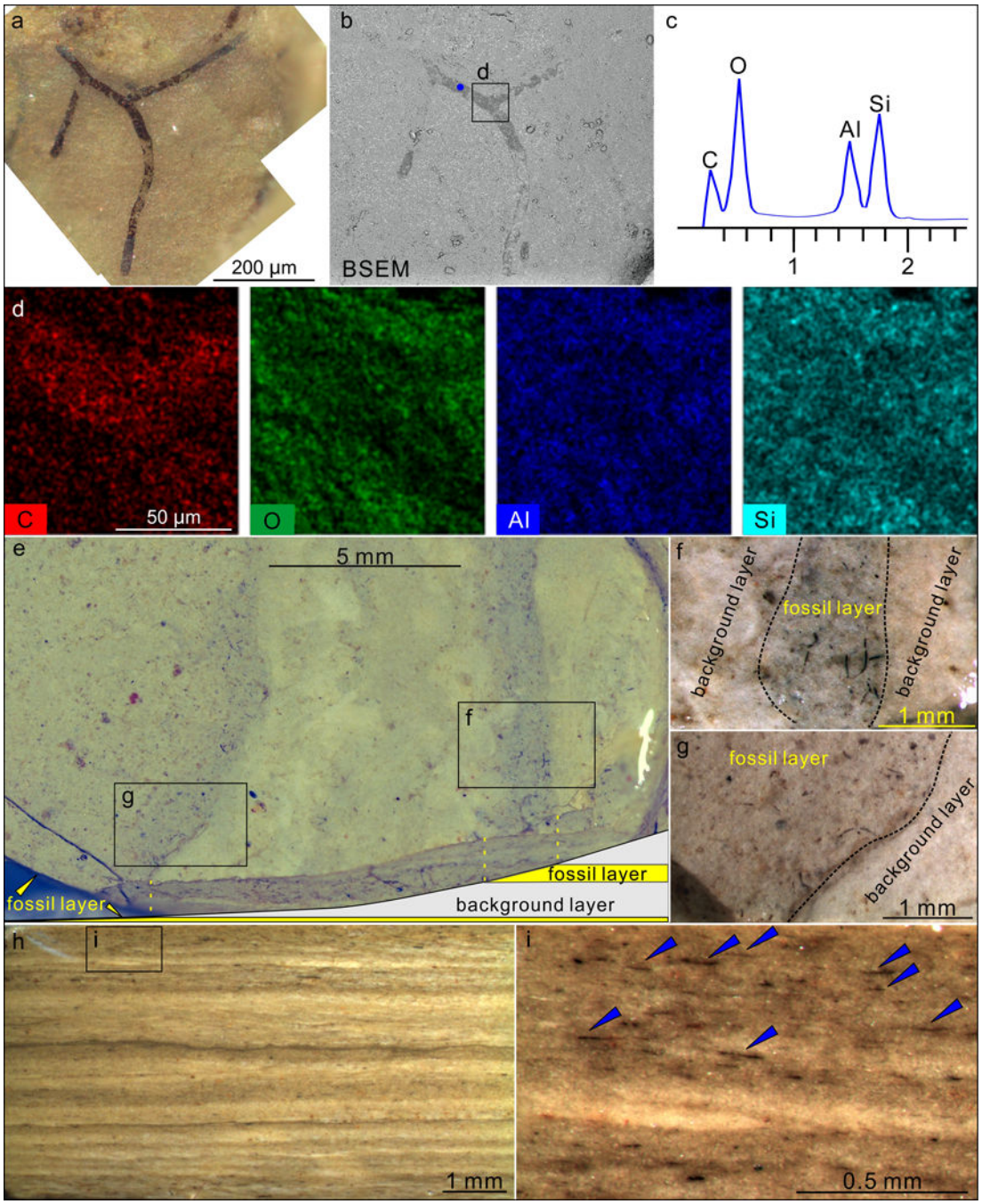

Extended Data Fig. 9. Taphonomy of *P. antiquus* preserved in the Nanfen mudstone.

a–**b**, A partially exposed specimen. **b** is a backscattered electron scanning electron microscopy (BSEM) photograph of the same specimen in **a**. VPIGM-4794. **c**, Energy dispersive X-ray spectroscopy (EDS) point analysis at the blue spot in **b**, showing the presence of carbon in the fossil specimen. **d**, EDS elemental maps of labeled box in **b**, showing the enrichment in C and deficiency in O, Al, and Si in fossil relative to matrix. **e**–**g**, Nanfen mudstone fractured obliquely relative to bedding plane, showing darker-colored fossil layers and lighter-colored background layers. **f** and **g** are magnifications of labeled

boxes in **e**. **h–i,** Polished slab cut perpendicular to bedding surface, showing darker-colored fossil layers and lighter-colored background layers. **i** is a close-up view of labeled box in **h** with blue arrowheads denoting fragmented fossils in a fossil layer. All photos taken by authors.

Supplementary Material

Refer to Web version on PubMed Central for supplementary material.

Acknowledgements

S.X. and Q.T. were supported by NASA Exobiology and Evolutionary Biology (80NSSC18K1086). X.Y. and K.P. were supported by National Natural Science Foundation of China (41602007), Chinese Academy of Sciences (QYZDJ-SSW-DQC009 and XDB 26000000), National Key Research and Development Program of China (2017YFC0603100), Science Foundation of Jiangsu Province of China (BK20161090), and State Key Laboratory of Palaeobiology and Stratigraphy of the Nanjing Institute of Geology and Palaeontology (193126 and 20162109). We thank Jinlong Wang for field assistance.

References

1. Falkowski PG et al. The evolution of modern eukaryotic phytoplankton. Science 305, 354–360 (2004). [PubMed: 15256663]
2. Keeling PJ The Number, Speed, and Impact of Plastid Endosymbioses in Eukaryotic Evolution. Annu. Rev. Plant Biol 64, 583–607 (2013). [PubMed: 23451781]
3. Brocks JJ et al. The rise of algae in Cryogenian oceans and the emergence of animals. Nature 548, 578–581 (2017). [PubMed: 28813409]
4. Knoll AH, Summons RE, Waldbauer JR & Zumberge JE in Evolution of Primary Producers in the Sea (eds Falkowski Paul G.& Knoll Andrew H.) 133–163 (Academic Press, 2007).
5. Parfrey LW, Lahr DJG, Knoll AH & Katz LA Estimating the timing of early eukaryotic diversification with multigene molecular clocks. Proc. Natl. Acad. Sci. USA 108, 13624–13629 (2011). [PubMed: 21810989]
6. Sánchez-Baracaldo P., Raven JA, Pisani D. & Knoll AH Early photosynthetic eukaryotes inhabited low-salinity habitats. Proc. Natl. Acad. Sci. USA 114, E7737–E7745 (2017). [PubMed: 28808007]
7. Gibson TM et al. Precise age of Bangiomorpha pubescens dates the origin of eukaryotic photosynthesis. Geology 46, 135–138 (2017).
8. Fučíková K. et al. New phylogenetic hypotheses for the core Chlorophyta based on chloroplast sequence data. Front. Ecol. Evol 2, article 63 (2014).
9. Jackson C., Knoll AH, Chan CX & Verbruggen H. Plastid phylogenomics with broad taxon sampling further elucidates the distinct evolutionary origins and timing of secondary green plastids. Sci. Rep 8, 1523 (2018). [PubMed: 29367699]
10. Del Cortona A. et al. Neoproterozoic origin and multiple transitions to macroscopic growth in green seaweeds. Proc. Natl. Acad. Sci. USA 10.1073/pnas.1910060117 (2020).
11. Berney C. & Pawlowski J. A molecular time-scale for eukaryote evolution recalibrated with the continuous microfossil record. Proc. R. Soc. B 273, 1867–1872 (2006).
12. Verbruggen H. et al. A multi-locus time-calibrated phylogeny of the siphonous green algae. Mol. Phylogenet. Evol 50, 642–653 (2009). [PubMed: 19141323]
13. Morris JL et al. The timescale of early land plant evolution. Proc. Natl. Acad. Sci. USA 115, E2274–E2283 (2018). [PubMed: 29463716]
14. Bengtson S., Sallstedt T., Belivanova V. & Whitehouse M. Three-dimensional preservation of cellular and subcellular structures suggests 1.6 billion-year-old crown-group red algae. PLOS Biol. 15, e2000735 (2017).
15. Betts HC et al. Integrated genomic and fossil evidence illuminates life's early evolution and eukaryote origin. Nat. Ecol. Evol 2, 1556–1562 (2018). [PubMed: 30127539]

16. Xiao S. et al. The Weng'an biota and the Ediacaran radiation of multicellular eukaryotes. Nati. Sci. Rev 1, 498–520 (2014).
17. Butterfield NJ, Knoll AH & Swett K. Paleobiology of the Neoproterozoic Svanbergfjellet Formation, Spitsbergen. Fossils Strata 34, 1–84 (1994).
18. Graham LE Digging deeper: why we need more Proterozoic algal fossils and how to get them. J. Phycol 55, 1–6 (2019). [PubMed: 30270424]
19. Marshall CR Confidence Intervals on Stratigraphic Ranges. Paleobiology 16, 1–10 (1990).
20. Zumberge JA, Rocher D. & Love GD Free and kerogen-bound biomarkers from late Tonian sedimentary rocks record abundant eukaryotes in mid-Neoproterozoic marine communities. Geobiology 10.1111/gbi.12378 (2019).
21. Gueneli N. et al. 1.1-billion-year-old porphyrins establish a marine ecosystem dominated by bacterial primary producers. Proc. Natl. Acad. Sci. USA 115, E6978–E6986 (2018). [PubMed: 29987033]
22. Hoshino Y. et al. Cryogenian evolution of stigmasteroid biosynthesis. Sci. Adv 3, e1700887 (2017).
23. Zhang S-H, Zhao Y., Ye H. & Hu G-H Early Neoproterozoic emplacement of the diabase sill swarms in the Liaodong Peninsula and pre-magmatic uplift of the southeastern North China Craton. Precambrian Res. 272, 203–225 (2016).
24. Bureau of Geology and Mineral Resources of Liaoning Province. Regional Geology of Liaoning Province. Chinese Ministry of Geology and Mineral Resources, Geological Memoris, series 1, number 5. 856 (Geological Publishing House, 1989).
25. Yang D-B et al. U-Pb ages and Hf isotope data from detrital zircons in the Neoproterozoic sandstones of northern Jiangsu and southern Liaoning Provinces, China: Implications for the late Precambrian evolution of the southeastern North China Craton. Precambrian Res. 216–219, 162–176 (2012).
26. Zhao H. et al. New geochronologic and paleomagnetic results from early Neoproterozoic mafic sills and late Mesoproterozoic to early Neoproterozoic successions in the eastern North China Craton, and implications for the reconstruction of Rodinia. Geol. Soc. Am. Bull 10.1130/B35198.1 (2019).
27. Pascher A. Uber Flagellaten und Algen. Ber. der Deutsch. Bot. Ges 32, 136–160 (1914).
28. Mattox KR & Stewart KD in Systematics of the Green Algae (Systematics Association Special Volume No. 27) (eds Irvine DEG & John DM) 29−72 (Academic Press, 1984).
29. Oltmanns F. Morphologie und Biologie der Algen. Vol. 1 733 (Gustav Fischer, 1904).
30. Zhao Z-J, Zhu H., Liu G-X & Hu Z-Y Rhizoclonium ramosum sp. nov. (Cladophorales, Chlorophyta), a new freshwater algal species from China. Fottea 16, 12–21 (2016).
31. Zhu H. et al. Molecular phylogeny and morphological diversity of inland Cladophora (Cladophorales, Ulvophyceae) from China. Phycologia 57, 191–208 (2018).
32. Okuda K. et al. Segregative cell division and the cytoskeleton in two species of the genus Struvea (Cladophorales, Ulvophyceae, Chlorophyta). Phycol. Res 64, 219–229 (2016).
33. Leliaert F. & Coppejans E. A revision of Cladophoropsis Børgesen (Siphonocladales, Chlorophyta). Phycologia 45, 657–679 (2006).
34. Hermann TN & Podkovyrov VN A discovery of Riphean heterotrophs in the Lakhanda Group of Siberia. Paleontol. J 44, 374–383 (2010).
35. Hermann TN Filamentous microorganisms in the Lakhanda Formation on the Maya River. Paleontol. J 1981(2), 100–107 (1981).
36. Nowak H. et al. Filamentous eukaryotic algae with a possible cladophoralean affinity from the Middle Ordovician Winneshiek Lagerstätte in Iowa, USA. Geobios 50, 303–309 (2017).
37. Wellman CH & Strother PK The terrestrial biota prior to the origin of land plants (embryophytes): a review of the evidence. Palaeontology 58, 601–627 (2015).
38. Nagovitsin KE et al. Revised Neoproterozoic and Terreneuvian stratigraphy of the Lena-Anabar Basin and north-western slope of the Olenek Uplift, Siberian Platform. Precambrian Res. 270, 226–245 (2015).

39. Xiao S. & Tang Q. After the boring billion and before the freezing millions: evolutionary patterns and innovations in the Tonian Period. Emerg. Top. Life Sci 2, 161–171 (2018). [PubMed: 32412616]
40. Fryxell GA Survival Strategies of the Algae. 144 (Cambrian University Press, 1983).
41. Komárek J. & Johansen JR in Freshwater Algae of North America (Second Edition) (eds Wehr John D., Sheath Robert G., & Kociolek J. Patrick) 135–235 (Academic Press, 2015).
42. Bartley JK Actualistic taphonomy of cyanobacteria: Implications for the Precambrian fossil record. Palaios 11, 571–586 (1996).
43. Niklas KJ & Newman SA The origins of multicellular organisms. Evol. and Dev 15, 41–52 (2013).
44. Roper M., Ellison C., Taylor John W. & Glass NL Nuclear and Genome Dynamics in Multinucleate Ascomycete Fungi. Curr. Biol 21, R786–R793 (2011). [PubMed: 21959169]
45. Randhawa MS Akinete formation in Vaucheria geminata. Bot. Gaz 103, 809–811 (1942).
46. Duffield ECS, Waaland SD & Cleland R. Morphogenesis in the red alga, Griffithsia pacifica: Regeneration from single cells. Planta 105, 185–195 (1972). [PubMed: 24477805]
47. Deacon J. Fungal Biology 4th edition. 371 (Blackwell Publishing Ltd, 1997).
48. Willetts HJ & Wong AL Ontogenetic diversity of sclerotia of Sclerotinia sclerotiorum and related species. Trans. Br. Mycol. Soc 57, 515–524 (1971).
49. Butterfield NJ A vaucheriacean alga from the middle Neoproterozoic of Spitsbergen: Implications for the evolution of Proterozoic eukaryotes and the Cambrian explosion. Paleobiology 30, 231–252 (2004).
50. Graham LE & Wilcox LE Algae. 640 (Prentice-Hall, 2000).
51. Butterfield NJ Bangiomorpha pubescens n. gen., n. sp.: Implications for the evolution of sex, multicellularity, and the Mesoproterozoic-Neoproterozoic radiation of eukaryotes. Paleobiology 26, 386–404 (2000).
52. Shih PM & Matzke NJ Primary endosymbiosis events date to the later Proterozoic with cross-calibrated phylogenetic dating of duplicated ATPase proteins. Proc. Natl. Acad. Sci. USA 110, 12355–12360 (2013). [PubMed: 23776247]
53. Moczydlowska M., Landing E., Zang W. & Palacios T. Proterozoic phytoplankton and timing of Chlorophyte algae origins. Palaeontology 54, 721–733 (2011).
54. Butterfield NJ Proterozoic photosynthesis – a critical review. Palaeontology 58, 953–972 (2015).
55. Knoll AH Paleobiological perspectives on early eukaryotic evolution. Cold Spring Harb. Perspect. Biol 6, a016121 (2014).
56. Butterfield NJ Early evolution of the Eukaryota. Palaeontology 58, 5–17 (2015).
57. Leliaert F. et al. Phylogeny and molecular evolution of the green algae. Crit. Rev. Plant Sci 31, 1–46 (2012).
58. Fang L., Leliaert F., Zhang Z-H, Penny D. & Zhong B-J Evolution of the Chlorophyta: Insights from chloroplast phylogenomic analyses. J. Syst. Evol 55, 322–332 (2017).
59. Cocquyt E., Verbruggen H., Leliaert F. & De Clerck O. Evolution and cytological diversification of the green seaweeds (Ulvophyceae). Mol. Biol. Evol 27, 2052–2061 (2010). [PubMed: 20368268]
60. Umen JG Green algae and the origins of multicellularity in the plant kingdom. Cold Spring Harb. Perspect. Biol 6, a016170 (2014).
61. Butterfield NJ Oxygen, animals and aquatic bioturbation: An updated account. Geobiology 16, 3–16 (2018). [PubMed: 29130581]
62. Gold DA et al. Sterol and genomic analyses validate the sponge biomarker hypothesis. Proc. Natl. Acad. Sci. USA 113, 2684–2689 (2016). [PubMed: 26903629]
63. Zumberge JA et al. Demosponge steroid biomarker 26-methylstigmastane provides evidence for Neoproterozoic animals. Nat. Ecol. Evol 2, 1709–1714 (2018). [PubMed: 30323207]
64. Bunt JS in Primary Productivity of the Biosphere (eds Lieth H. & Whittaker RH) 169–183 (Springer, 1975).
65. Loron CC et al. Early fungi from the Proterozoic era in Arctic Canada. Nature 570, 232–235 (2019). [PubMed: 31118507]

66. Schuster A. et al. Divergence times in demosponges (Porifera): first insights from new mitogenomes and the inclusion of fossils in a birth-death clock model. BMC Evol. Biol 18, 114 (2018). [PubMed: 30021516]

67. Cole DB et al. A shale-hosted Cr isotope record of low atmospheric oxygen during the Proterozoic. Geology 7, 555–558 (2016).

68. Tsutsui I. et al. Ecological and Morphological Profile of Floating Spherical Cladophora socialis Aggregations in Central Thailand. PLOS ONE 10, e0124997 (2015).

69. Parial D. & Pal R. Biosynthesis of monodisperse gold nanoparticles by green alga Rhizoclonium and associated biochemical changes. J. Appl. Phycol 27, 975–984 (2015).

70. Zhao Z-J, Zhu H., Hu Z-Y & Liu G-X Occurrence of true branches in Rhizoclonium (Cladophorales, Ulvophyceae) and the reinstatement of Rhizoclonium pachydermum Kjellman. Phytotaxa 166, 273–284 (2014).

71. Tang Q. et al. Organic-walled microfossils from the early Neoproterozoic Liulaobei Formation in the Huainan region of North China and their biostratigraphic significance. Precambrian Res. 236, 157–181 (2013).

72. Wang Y., Xu H-H, Wang Y. & Fu Q. A further study of Zosterophyllum sinense Li and Cai (Zosterophyllopsida) based on the type and the new specimens from the Lower Devonian of Guangxi, southwestern China. Rev. Palaeobot. Palyno 258, 112–122 (2018).

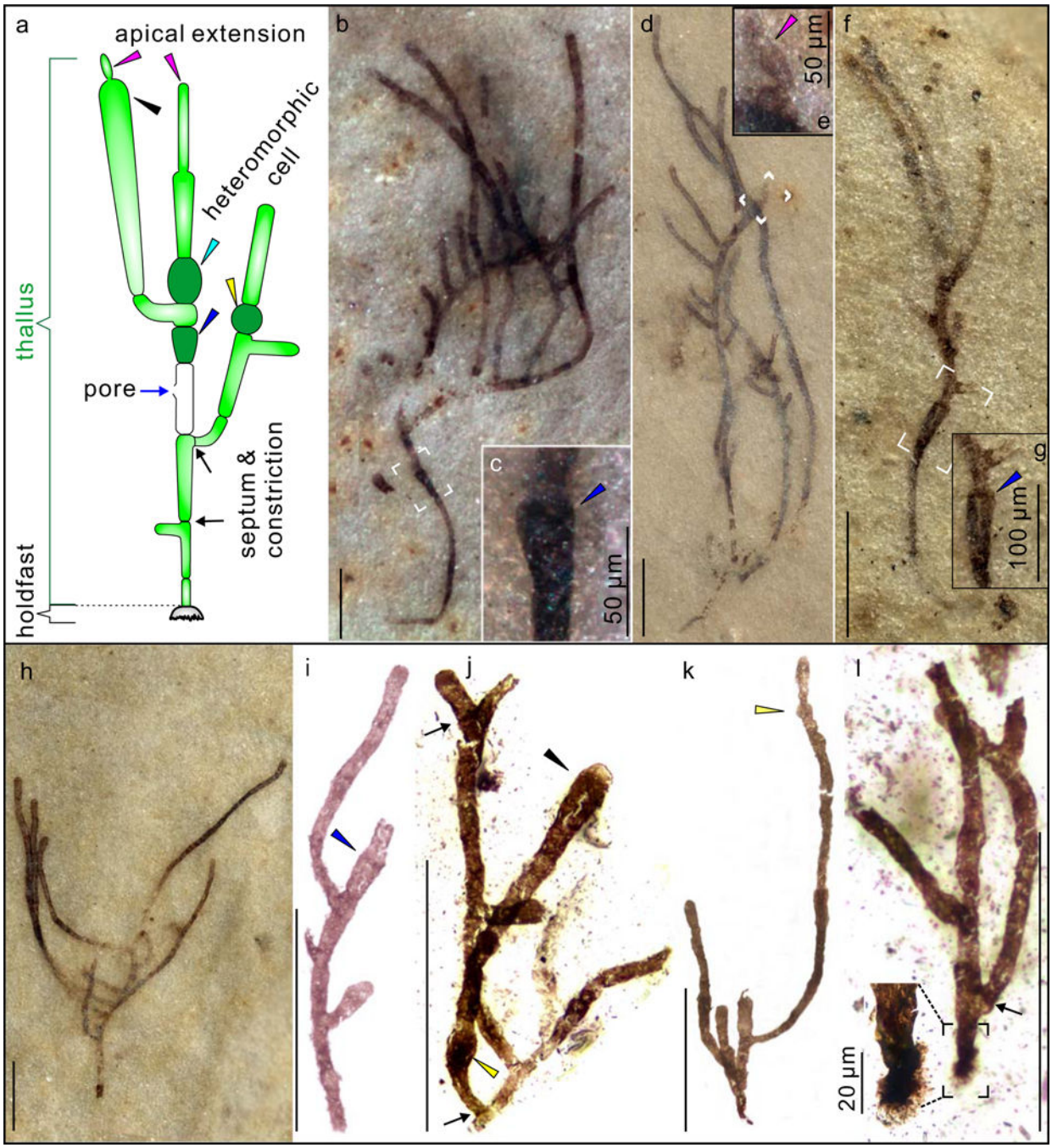

Figure 1 |. Gross morphology of *Proterocladus antiquus* new species from the Nanfen Formation. **a**, Morphological reconstruction and terminology. **b–h**, Slender thalli preserved on bedding surfaces. **c**, **e**, and **g** are magnifications of white frames in **b**, **d**, and **f**, respectively, showing cyathiform heteromorphic cells (in **c** and **g**) and apical extension (in **e**). VPIGM-4749, VPIGM-4750, VPIGM-4751, and VPIGM-4752, respectively. **i–l**, Branching thalli extracted from rock matrix using HF acid maceration technique. A close-up view is provided for the holdfast in the black frame in **l**. VPIGM-4753, VPIGM-4754, VPIGM-4755, and VPIGM-4799 (paratype), respectively. Blue arrowheads in **a**, **c**, **g**, and **i:** cyathiform

heteromorphic cell; purple arrowheads in **a** and **e:** apical extension; black arrowheads in **a** and **j:** clavate cell; yellow arrowheads in **a**, **j**, and **k:** globose heteromorphic cell; black arrows in **a**, **j**, and **l**: septum and constriction. Scale bars equal 200 μm unless otherwise specified. All photos taken by authors.

Figure 2 |. Cellular structures of *Proterocladus antiquus* new species.

a–f, Fragmentary specimens extracted from rock matrix using HF acid maceration technique. VPIGM-4756, VPIGM-4757, VPIGM-4758, VPIGM-4759, VPIGM-4760, and VPIGM-4761, respectively. **g–k**, Well-preserved thallus on bedding surface. VPIGM-4762 (holotype). **h–k** are magnifications of labeled frames in **g**. Black and blue arrows denote robust septa and lateral pore, respectively. Cyan, blue, and purple arrowheads denote morphologically differentiated doliform hetermorphic cells, cyathiform hetermorphic cells,

and narrow apical extensions, respectively. Scale bars equal 100 μm unless otherwise specified. All photos taken by authors.

Figure 3 |. Extant Siphonocladales of the genera *Cladophora* and *Rhizoclonium* for comparison with *Proterocladus*.

a, General morphology of a branching thallus of *Cladophora*, showing elongate cells and unique lateral branching system. Compare with Fig. 1b, d. **b**, Doliform akinetes (cyan arrowheads) of *Rhizoclonium* under stressed conditions in contrast to the cylindrical vegetative cells (white arrowhead). Compare with Fig. 2f. **c**, Reproductive cells of *Rhizoclonium* with lateral pore (white arrows) after the liberation of gametes or zoospores. Compare with Fig. 2e. **d**, Lateral branches (blue arrowheads) of *Cladophora* arising from mother cell subjacent to septa and remaining cytoplasmic contact with mother cell. Compare with Fig. 2a. **a** adapted from ref.[68] under a Creative Commons License, **b** from ref.[69] with permission, **c** from ref.[70] under a Creative Commons License, and **d** from ref.[31] with permission.

Figure 4 |.
An artist's reconstruction of *Proterocladus antiquus*. Artwork by Dinghua Yang.